DOI: 10.61782/fa.2025.0495

FORUM ACUSTICUM EURONOISE 2025

ON THE RELATIONSHIPS BETWEEN MANUFACTURING PARAMETERS, GEOMETRICAL ACCURACY, AND VIBRATIONAL PROPERTIES OF SELECTIVE LASER SINTERED PA-12 BEAMS

Kryuchkov A.[1,2*] **Pavan M.**[1] **Claeys C.**[2,4] **Deckers E.**[3,4]

[1] Materialise NV, Leuven, Belgium
[2] Department of Mechanical Engineering, KU Leuven, Belgium
[3] Department of Mechanical Engineering, Diepenbeek, KU Leuven, Belgium
[4] Flanders Make @ KU Leuven, Belgium

ABSTRACT

Selective Laser Sintering (SLS) enables the production of complex structures, but ensuring their geometrical accuracy and material properties remains challenging due to many parameters that influence the final print quality. This study investigates the vibrational properties of PA-12 beams manufactured using SLS, focusing on the relationships between the manufacturing parameters, geometrical accuracy, and natural frequencies. The beams are evenly distributed across the build volume to investigate spatial and thermal effects on the quality of the part. Dimensional measurements are used to calculate the expected natural frequencies of the cantilever beams, which are then compared with the experimental results obtained using an automated impact hammer setup. The collected data visualizes the relationships between beam dimensions, resonant frequencies, and temperature of the printer bed. This data can further be used to optimize SLS manufacturing parameters for improved precision and mechanical performance of printed components, especially important in the design and reliable performance of produced metamaterials, where small deviations can significantly alter functional behavior.

**Corresponding author*:
alexander.kryuchkov@materialise.be.

Keywords: *Selective Laser Sintering, PA-12, Natural Frequencies, Additive Manufacturing Accuracy, Metamaterials*

1. INTRODUCTION

Selective Laser Sintering (SLS) is a powder bed additive manufacturing (AM) process that uses one or more lasers to selectively fuse polymer powder layer by layer, enabling the fabrication of complex self-supporting geometries without the need for molds or support structures [1, 2]. Polyamide-12 (PA-12) is a common SLS material valued for its mechanical properties. Achieving high dimensional accuracy in SLS parts is critical, as deviations can negatively impact both mechanical and functional performance [2].

However, maintaining this accuracy is challenging because of shrinkage and warping effects. These occur when the sintered layers cool and crystallize, resulting in geometric distortions [3]. Effective thermal management is therefore essential to mitigate these effects and ensure consistent replication of the intended design dimensions [3, 4]. Such precision becomes even more important in acoustically sensitive designs, where geometric inaccuracies can degrade performance. For example, a study of 3D printed air diffusers found that differences in surface quality and dimensional precision across AM methods significantly influenced acoustic performance [5]. Accurate part fabrication is therefore essential in acoustic applications that rely on tightly controlled geometries. An explicit link is made between the production accuracy of

SLS and the resulting vibro-acoustic properties in a study of a lightweight vibro-acoustic metamaterial demonstrator [6]. In another investigation focused on acoustic resonators, it is suggested that the deviation of the experimental results from the predicted peaks (theory and FEA) might have been caused by geometrical inaccuracies of the 3D-printing machine [7]. Additionally, surface roughness introduced during additive manufacturing has been shown to significantly affect acoustic performance [8]. There is also growing interest in using 3D printed structures for vibration and modal analysis [9].

This study investigates the vibrational performance of PA-12 cantilever beams fabricated across the SLS build volume. Specifically, it examines how dimensional variations and thermal history correlate with the natural frequencies of the beams. The objective is to determine whether certain process parameters significantly influence resonance behavior. This information could accelerate quality control processes in the future.

2. METHODS

2.1 Part Fabriction

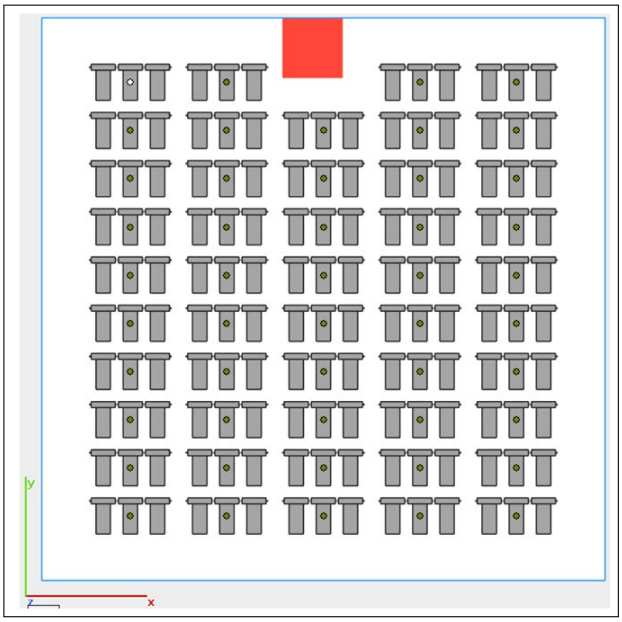

Figure 1. Top view of the printer bed beam layout.

The cantilever beam parts were manufactured using SLS on a Sindoh S100 laser sintering system. Each printed unit consists of three beam segments connected by a thin cylindrical bridge with a diameter of 1.5 mm. The base section of each beam is designed as a 5 × 5 × 20 mm³ block, while the beam portion extends 25 mm in length, 12 mm in width, and 2.5 mm in thickness. These dimensions are shown in millimeters in Figure 2.

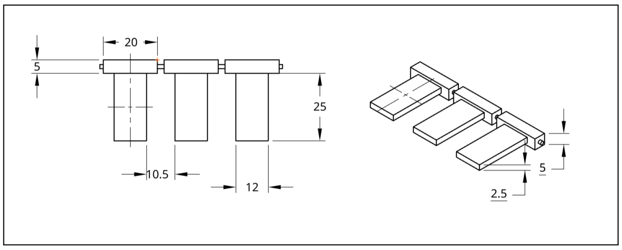

Figure 2. Dimensions of the beam set (mm).

To investigate spatial effects on part quality, the beam units were distributed evenly across the build volume. Individually, the beams form a 15 × 10 grid, which is stacked vertically for a total of 10 layers along the Z-axis. A margin of approximately 40 mm was maintained on all four sides of the print bed. Additionally, a 10 mm vertical offset was introduced below the first printed layer to help record thermal history. The spacing between adjacent parts was 12.5 mm in the X-direction, 10 mm in the Y-direction, and 20 mm in the Z-direction. Figure 1 illustrates the layout of the beam units on the printer bed. The red square in the rear region of the bed denotes a "no-build zone", designated for pyrometer temperature measurements.

All parts were printed in a single job using the same process parameters. A 1:1 mix of new and recycled PA-12 powder was used, with the bed preheat temperature maintained at 173°C. Although the print order reflects the digital label of a part, the actual scan pattern generally proceeded from the front-left to the back-right corner of the print bed, with the back row typically completed last within each layer. Upon completion, the build was allowed to cool gradually inside the chamber for four days.

All beams were labeled at the base, corresponding to their location. All three beam parts in one unit have the same X,Y, and Z label, and are distinguished by an additional number, i.e, X1Y2Z3B1, X1Y2Z3B2 and X1Y2Z3B3 with XYZ referring to the position of the unit in the build.

2.2 Geometrical Measurements

Only beams located in the odd-numbered Z-layers were measured. The primary dimensions — length, width, and thickness — were recorded using digital calipers. All measurements were taken at consistent locations across the parts. Length was measured once along the centerline of the beam (Figure 2, from base to tip. Additional measurements from the base to the left and right sides of the tip were also taken, however, only the central full-length measurement was used in the data analysis due to its greater reliability.

Width and thickness were each measured at three positions along the beam: near the base, at the midpoint, and near the tip. The centerline is shown as a dashed line in Figure 2. For data processing, the average of the midpoint and near-tip measurements was used. Measurements taken near the base were excluded from the average due to greater potential for deviation, as that region is influenced by proximity to the part's base feature.

2.3 Thermal Monitoring

The printer bed temperature was recorded using two instruments located inside the printer: the Optris CT LT pyrometer and the FLIR A655sc infrared (IR) camera. A custom script logged temperature data twice per layer: once before scanning and once before recoating the new layer. The pyrometer readings were used to correct the IR images, as the IR camera is more susceptible to heat deviations and artifacts. Each IR image was subsequently processed to determine the average temperature in the area surrounding each beam. Each beam had a square region positioned at its center, encompassing both the beam itself and the surrounding area on either side. The average temperature was then determined by averaging the pixel values within this selected square region. Certain spots were excluded from the analysis due to obstructions or dead pixels in the IR camera.

2.4 Vibrational Testing

Natural frequencies were extracted using the Grindosonic MK7 automatic impact hammer testing setup. Each beam was positioned on a piece of soft foam, placed directly above the microphone of the device. The impact hammer delivered a consistent tap to the part of the beam corresponding to the expected location of maximum displacement in the first natural frequency mode. The test was repeated three times per beam to ensure repeatability. Only the beams from the first printed layer were measured.

3. RESULTS

The SLS process yielded relatively small dimensional deviations in the length and width of the beams. However, thickness exhibited significantly larger deviations, primarily due to the small design value of 2.5 mm and the influence of shrinkage and warpage effects, as discussed in Section 1. This comparison is illustrated in Figure 3. While length and width deviations were generally centered around 0%, thickness deviations were consistently positive, ranging from approximately 9% to 20%.

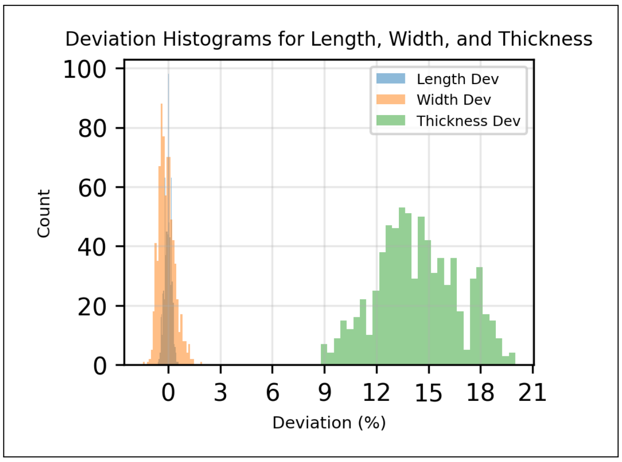

Figure 3. Percent deviation from the design values of beams' dimensions.

A closer look at the thickness distribution at layer Z3, shown in Figure 4, reveals that the thicker beams are concentrated on the right side, particularly near the back-right corner of the printer bed. This trend is also observable, to varying degrees, across the other measured layers.

Figure 5 shows the average temperature measured at each beam location. Uneven thermal distribution across the print bed is evident, with cooler temperatures concentrated near the center. In contrast, the highest recorded temperatures are observed near the back-right corner of the printer bed.

To compare thickness variations, Figures 6 and 7 display all thickness measurements plotted against their corresponding positions. Each data point is colored according to its print order. The front view in Figure 6 reveals an increase in thickness values from left to right, particularly noticeable in X indices 4 and 5. Figure 7 confirms

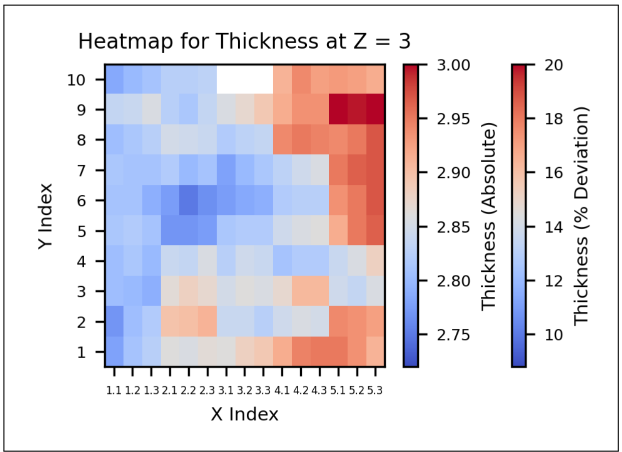

Figure 4. Heatmap of thickness measurements in layer Z3.

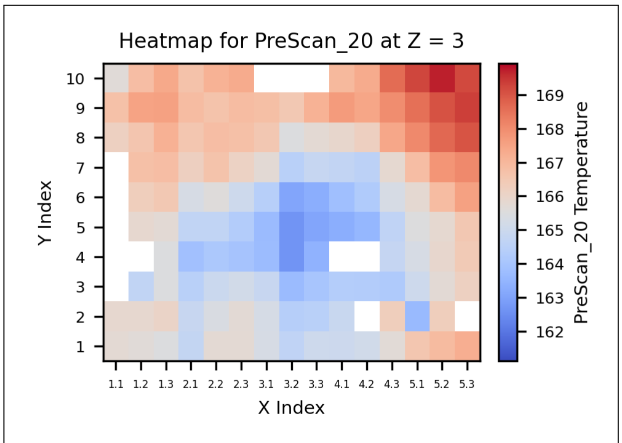

Figure 5. Heatmap of prescan temperature at the twentieth layer of parts at layer Z3 (obstructions and dead pixel measurements excluded).

that parts were generally printed from the front to the back of the bed and highlights a noticeable dip in thickness between Y indices 4 and 7.

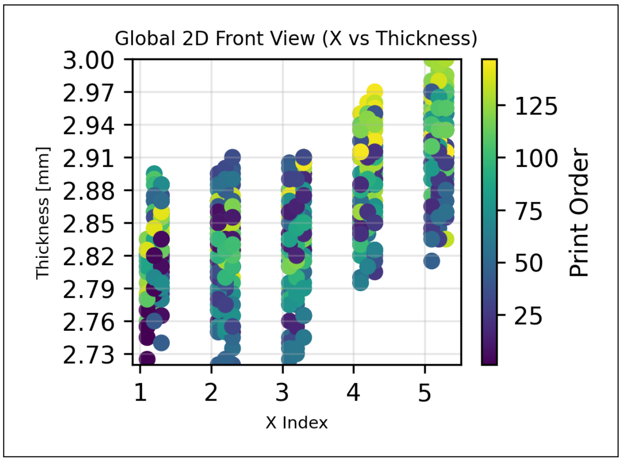

Figure 6. Front view of thickness measurements with print order in all measured layers.

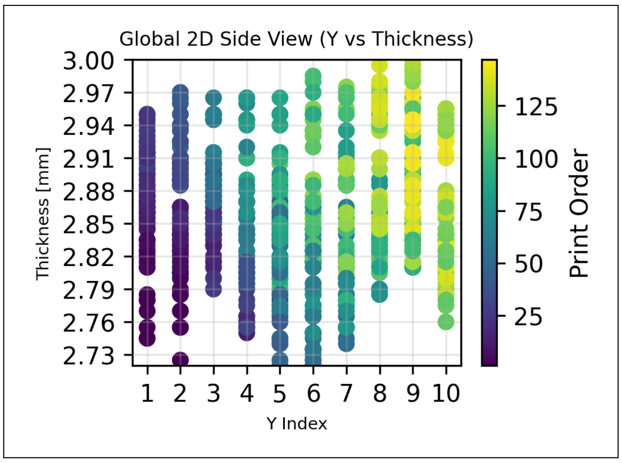

Figure 7. Side view of thickness measurements with print order in all measured layers.

Figure 8 presents the correlation matrix for all measured variables at layer Z1. In this figure, Interlayer T and Part T refer to the temperature measurements taken between layers and at the part layers, respectively. PR and PS denote the PreRecoat and PreScan processes. The numerical suffix indicates the layer number at the specific location: -1 corresponds to the layer just before the part is printed, while 20 indicates the twentieth layer of the part. Strong correlations are observed between the different temperature measurements, as well as between frequency and both width and thickness. Moderate correlations are also evident between temperature variables and beam dimensions, as well as with the print order.

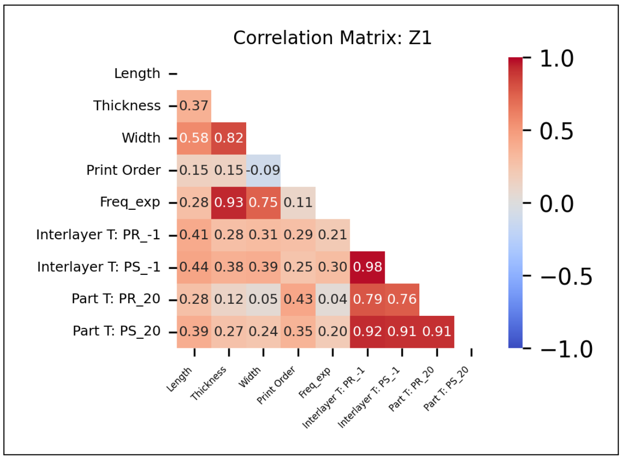

Figure 8. Correlation matrix of measurements in Z1.

The correlation matrix across all layers is shown in Figure 9, which excludes the frequency measurements. Compared to Figure 8, the correlations between the temperature variables, beam dimensions, and print order appear stronger when considering the full dataset. This suggests that the overall thermal history and printing sequence have a more pronounced effect on the geometry of the parts when aggregated across all layers.

4. DISCUSSION

The results of this study provide insights into the complex relationship between SLS manufacturing parameters, dimensional accuracy, and the vibrational properties of PA-12 parts.

4.1 Printer Bed Temperature

Goodridge et al. identified thermal management as one of the primary challenges in achieving consistent part quality in SLS processes [1]. The heatmap of the temperature distribution in Figure 5 shows a distinct thermal variation across the build platform: lower temperatures are observed near the center of the bed, while higher temperatures appear around this region, with the highest values recorded near the back-right corner. This uneven

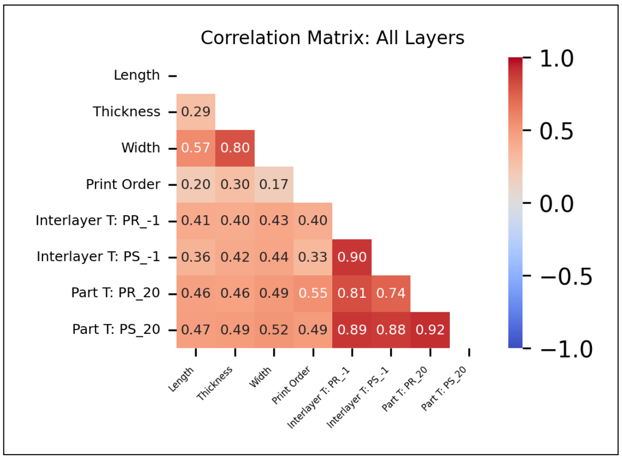

Figure 9. Correlation matrix of measurements in all measured layers.

heating correlates with observed variations in part dimensions. For instance, Figure 7 shows that beams located in the middle of the bed (Y5–Y7) tend to be thinner than those printed in surrounding regions. Likewise, Figure 4 indicates that the beams located in the back-right corner—where the temperatures are highest—are among the thickest in the build.

Despite this spatial trend, the correlation matrix in Figure 9 shows only moderate correlations between recorded temperatures and beam thickness. One explanation is that beams near the left edge of the build are also thinner, yet they experience similar temperature levels to those on the right. This suggests that additional factors, such as print order or local cooldown conditions, may play a role. As described in Section 2, the print order generally progresses from the front-left to the back-right corner, meaning the last-printed parts (often thicker) also correspond to areas with higher recorded temperatures. This may indicate a cumulative thermal effect, where successive laser passes raise the local bed temperature, influencing not only the printed layers but also the interlayers preceding them. However, if temperature were driven only by this effect, a stronger correlation with thickness would be expected. The moderate correlation observed likely arises because temperature is affected by both space and time factors. For instance, thin parts situated near the center of the bed may lie in regions with higher temperatures, but those parts are printed earlier within the layer sequence. As a result, the influence of geometry on temperature becomes entangled with location and print sequence, weakening the direct correlation between thickness and recorded temperature.

Additionally, the absolute temperature values in Figure 5 are notably lower than the target preheat temperature of 173°C. While the powder bed reaches this temperature during the interlayer heating phase, it drops rapidly during the printing of each layer due to the time required for sintering. The internal heaters cannot compensate quickly enough, resulting in lower effective temperatures at the printed layers. This drop appears to be specific to the part layout of this particular print job and setup – too many small parts were evenly distributed throughout the printer bed, which is not common in typical builds.

4.2 Parameter Correlations

The global correlation matrix in Figure 9 reveals several key relationships between print parameters and part quality. As discussed in Section 1, shrinkage and warpage are known to affect dimensional accuracy. In this design, the width and thickness were more sensitive to these effects and thus exhibited a strong correlation with one another.

Moderate correlations were observed between all temperature variables and both the geometric dimensions and print order. These findings are consistent with the analysis presented in Section 4.1, which suggests that localized temperature changes and thermal history contribute to dimensional variability.

In the Z1 correlation matrix shown in Figure 8, the natural frequency variable was included and, as expected, showed strong correlations with both thickness and width. This is in line with theoretical predictions: the first mode of vibration in beams is a bending mode, which strongly depends on the beam's moment of inertia I, defined for a rectangular cross-section as shown in Equation 1. Here, w is the beam width and t is the beam thickness (height in the bending direction). Dimensional deviations in these parameters therefore have a direct and significant effect on the measured vibrational behavior.

$$I = \frac{wt^3}{12} \tag{1}$$

The strong correlation between natural frequency and thickness and width suggests that frequency testing can serve as an effective quality control method on its own. Rather than relying on multiple dimensional measurements, a streamlined quality control process could use automated frequency testing to flag parts that deviate from expected resonant behavior. Since the natural frequency is highly sensitive to small geometric variations, setting specific frequency thresholds would allow rapid identification of parts that may not meet the required geometrical criteria. This non-destructive testing approach could substantially reduce inspection time and costs, ensuring that only components with the proper vibrational characteristics proceed to final assembly or application in acoustically sensitive systems.

5. CONCLUSION

This study has investigated the relationships between SLS manufacturing parameters, dimensional accuracy, and vibrational properties of PA-12 cantilever beams. The findings reveal variations in thickness throughout the build volume that moderately correlate with temperature in the powder bed. Correlation analysis of the first layer of printed beams demonstrated consistent relationships between thermal conditions, dimensional deviations, print order, and natural frequencies. A strong correlation between natural frequency and part dimensions suggests the possibility of a faster, geometry-based quality control process for SLS-manufactured PA-12 parts. While only moderate correlations were found between frequency and temperature data in the first layer, measuring additional layers may reveal stronger associations.

Several areas for improvement and further investigation have emerged. First, the part design should be revised. A revised design could improve the reliability of frequency measurements and potentially reduce scan times — an important factor, as prolonged scanning was observed to lower the bed temperature during printing.

Additionally, increasing the preheating duration may help stabilize the thermal environment. Uncorrected IR camera data showed that the machine was still accumulating heat during the first two part layers of the build. A longer preheating phase could allow the system to reach thermal equilibrium before the actual printing begins. Furthermore, re-evaluating the heater orientation within the machine may help achieve a more uniform temperature distribution across the build surface.

Future work should focus on a more comprehensive analysis of the interactions between process parameters, dimensional accuracy, and vibrational response. This includes collecting data across all build layers, improving thermal management, and optimizing beam geometry. The application of compensation factors to address predictable dimensional deviations could lead to improved part consistency and performance.

6. ACKNOWLEDGMENTS

We gratefully acknowledge the European Commission for its support of the Marie Sklodowska Curie program through the Horizon Europe DN METAVISION project (GA 101072415). Views and opinions expressed are however those of the authors only and do not necessarily reflect those of the European Union. The European Union cannot be held responsible for them. The authors thank the Grindosonic team for their support in collecting the frequency data. The first author also thanks Ricardo Santander, Stefan Janssen, and Piet Van den Ecker for their invaluable help and patience. Materialise's MatGPT text-generator was used to debug parts of the code used for this study.

7. REFERENCES

[1] R. D. Goodridge, C. J. Tuck, and R. J. M. Hague, "Laser sintering of polyamides and other polymers," *Progress in Materials Science*, vol. 57, pp. 229–267, 2012.

[2] A. E. Magri, S. E. Bencaid, H. R. Vanaei, and S. Vaudreuil, "Effects of laser power and hatch orientation on final properties of pa12 parts produced by selective laser sintering," *Polymers, 14, 3674*, 2022.

[3] J. Li, S. Yuan, J. Zhu, S. Li, and W. Zhang, "Numerical model and experimental validation for laser sinterable semi-crystalline polymer: Shrinkage and warping," *Polymers, 12(6), 1373*, 2020.

[4] A. Pilipović, P. Ilinčić, M. Tujmer, and M. R. Havstad, "Impact of part positioning along chamber z-axis and processing parameters in selective laser sintering on polyamide properties," *Appl. Sci., 14, 976.*, 2024.

[5] T. O. Joldos, P. Danca, and A. Cernei, "Comparative acoustic analysis of standard and innovative air diffusers with enhanced mixing capabilities," in *E3S Web Conf.*, vol. 608, 2025.

[6] C. Claeys, E. Deckers, B. Pluymers, and W. Desmet, "A lightweight vibro-acoustic metamaterial demonstrator: Numerical and experimental investigation," *Mechanical Systems and Signal Processing*, vol. 70, pp. 853–880, 2016.

[7] A. C. de Sousa, E. Deckers, C. Claeys, and W. Desmet, "On the assembly of archimedean spiral cavities for sound absorption applications: Design, optimization and experimental validation," *Mechanical Systems and Signal Processing*, vol. 147, p. 107102, 2021.

[8] A. Ciochon and J. Kennedy, "Efficient modelling of surface roughness effects in additively manufactured materials," *Applied Acoustics*, vol. 220, p. 109953, 2024.

[9] P. Boron, J. Chelmecki, J. M. Dulinska, N. Jurkowska, B. Ratajewicz, P. Stecz, and T. Tatara, "On the possibility of using 3d printed polymer models for modal tests on shaking tables: Linking material properties investigations, field experiments, shaking table tests, and fem modeling," *Materials (Basel), 16(4):1471*, 2023.